Supporting Information

Understanding nucleotide-regulated FtsZ filament dynamics and the monomer assembly switch with large-scale atomistic simulations

Erney Ramírez-Aportela[1,2], Jose Ramón López-Blanco[1], José Manuel Andreu[2], Pablo Chacón[1]

[1]Department of Biological Physical Chemistry, Instituto de Química-Física Rocasolano, CSIC, Serrano 119. 28006 Madrid.

[2]Department of Chemical and Physical Biology, Centro de Investigaciones Biológicas, CSIC, Ramiro de Maeztu, 9. 28040 Madrid.

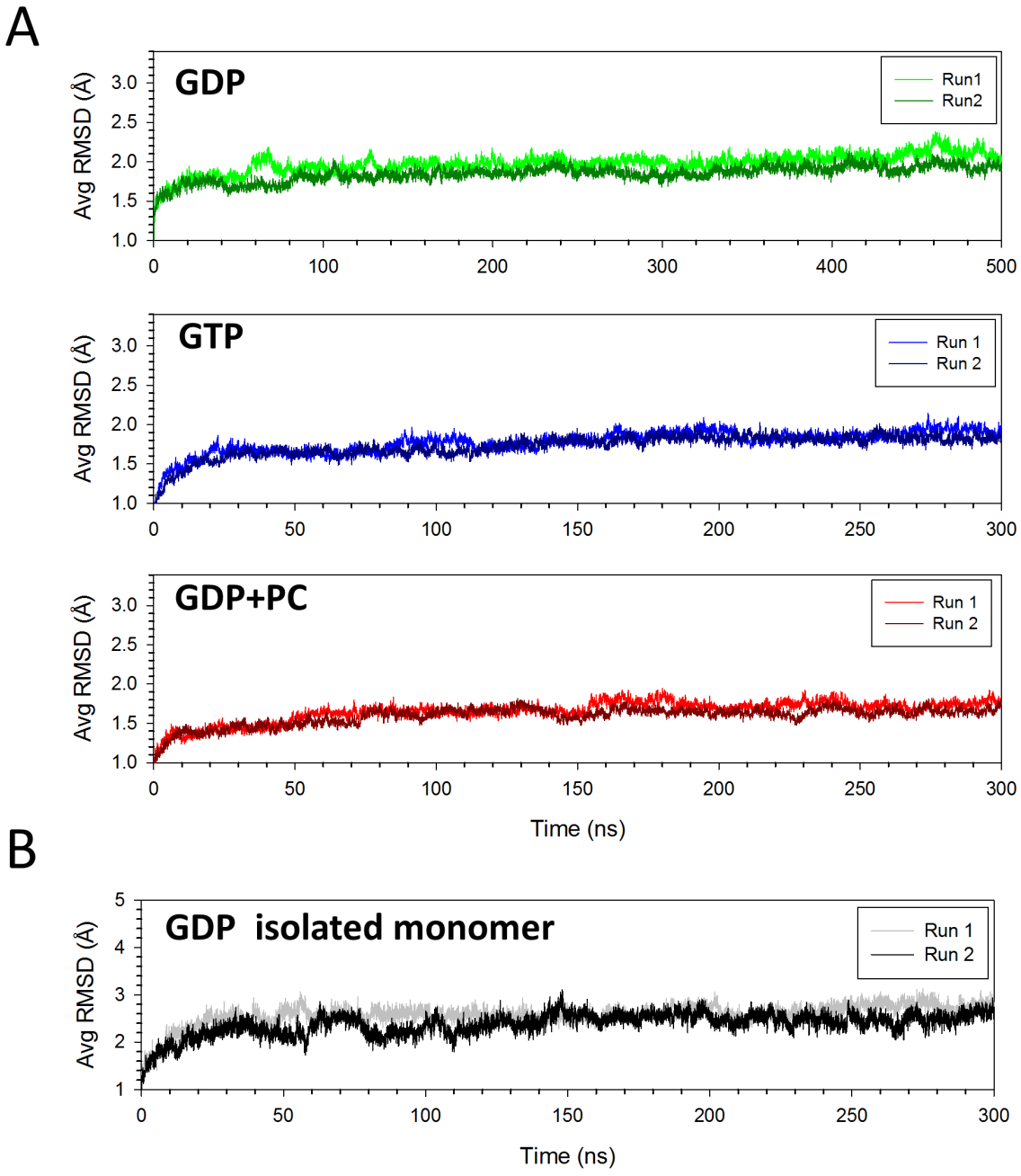

Figure S1. RMSD evaluated along the trajectories. (A) Average RMSD of the FtsZ monomers within the corresponding filaments along trajectories. The structures of the two end monomers have been excluded to avoid border effects, and two runs are plotted per case. (B) Average RMSD for the isolated GDP FtsZ monomer. In all the cases, the RMSD was computed considering backbone atoms using g_rmsd from GROMACS tools.

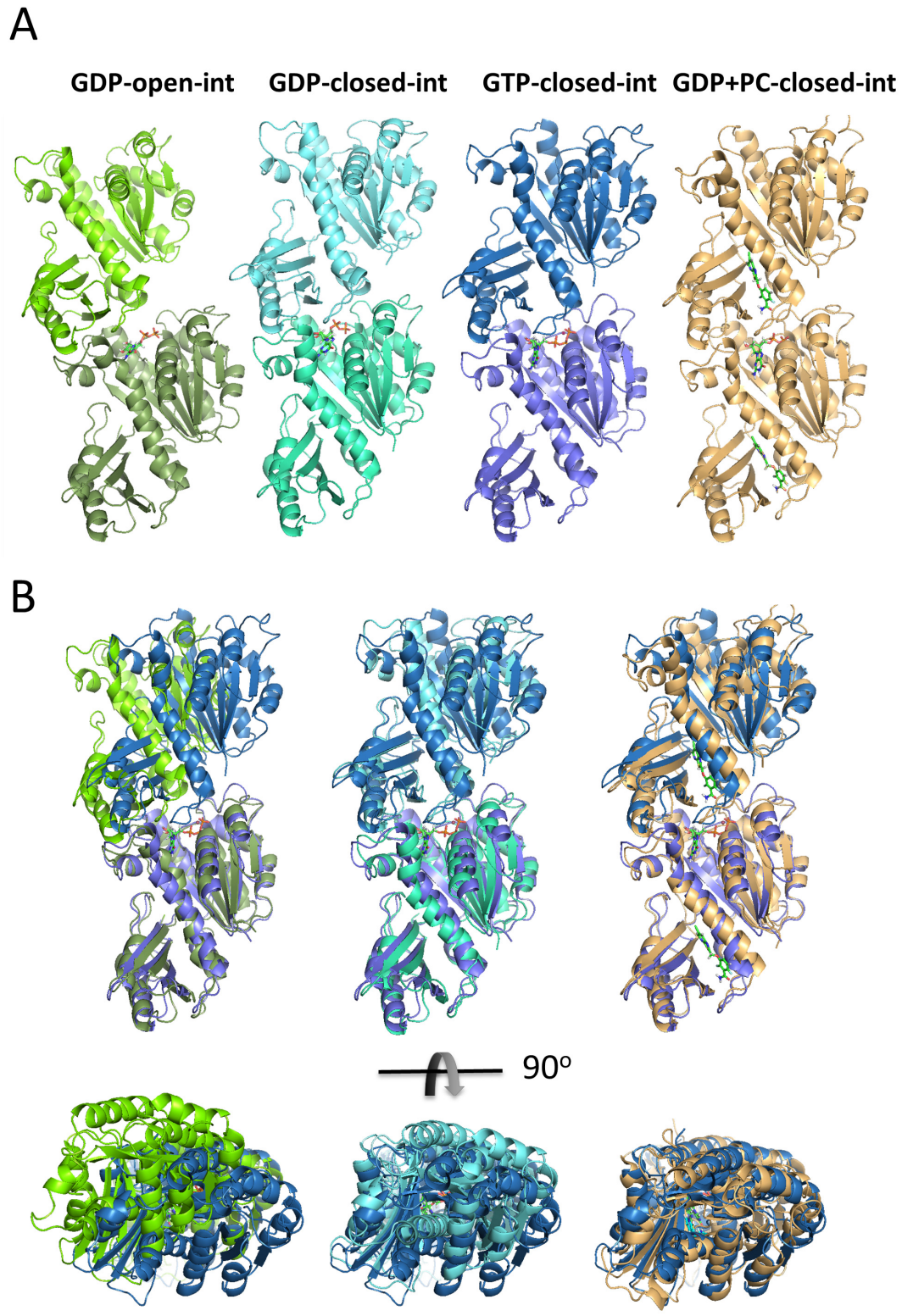

Figure S2. A. Illustrative dimer structures corresponding to GDP-open (green), GDP-closed (cyan), GTP (blue) and PC (wheat) monomer-to-monomer interfaces. B. Alignment of the GDP-open, GDP-closed and PC dimers with the GTP dimer.

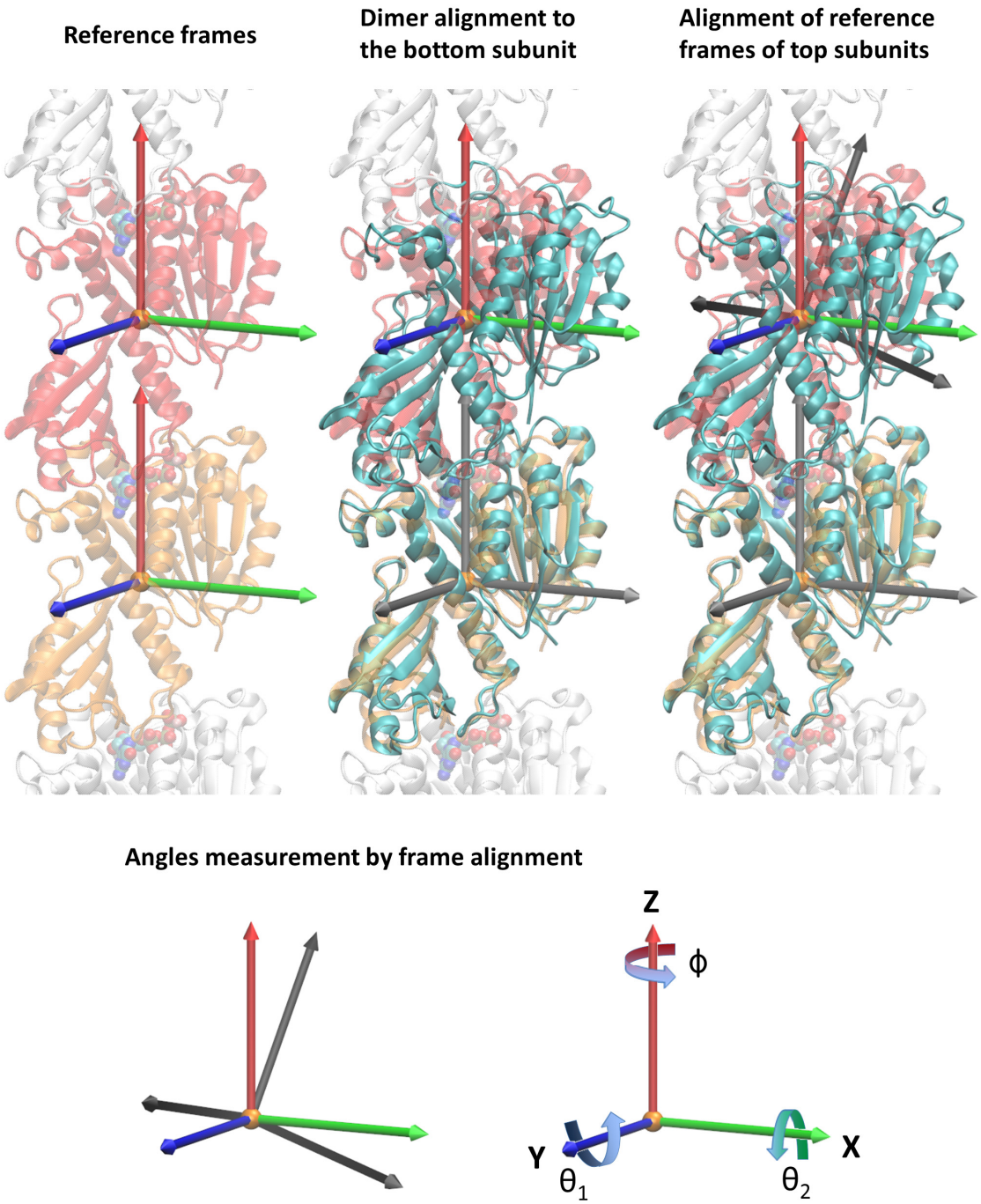

Figure S3. Definitions of bending and twisting angles. The relative orientation of each pair of monomers was monitored throughout the final 100 ns of the trajectories following a described methodology (1, 2). In brief, the coordinate frame was defined by aligning the z axis along the monomers' centers of mass, fixing the x axis along the direction of bending and defining an orthogonal y axis. For comparative proposes, the main bending angle $\theta_1$was set to lie in the maximal bending direction of the GTP filament. Rotations around the axes of the coordinate frame defined the bending and twisting angles that could be individually tracked for each monomer-monomer pair in the filaments, as depicted. To measure the angles, two consecutive monomers were first aligned with respect to the straight reference by superposing the bottom monomers. The corresponding bending angles are tracked by calculating the sequential rotations to align the coordinate reference frames of the top monomers. The bending angles θ_1 and θ_2 were defined by rotations around the Y axis (blue) and the X axis (green), respectively and the twist (Φ) was defined by the rotation around the Z axis (red). Note that this view is roughly equivalent to tubulin viewed from the inside of a microtubule.

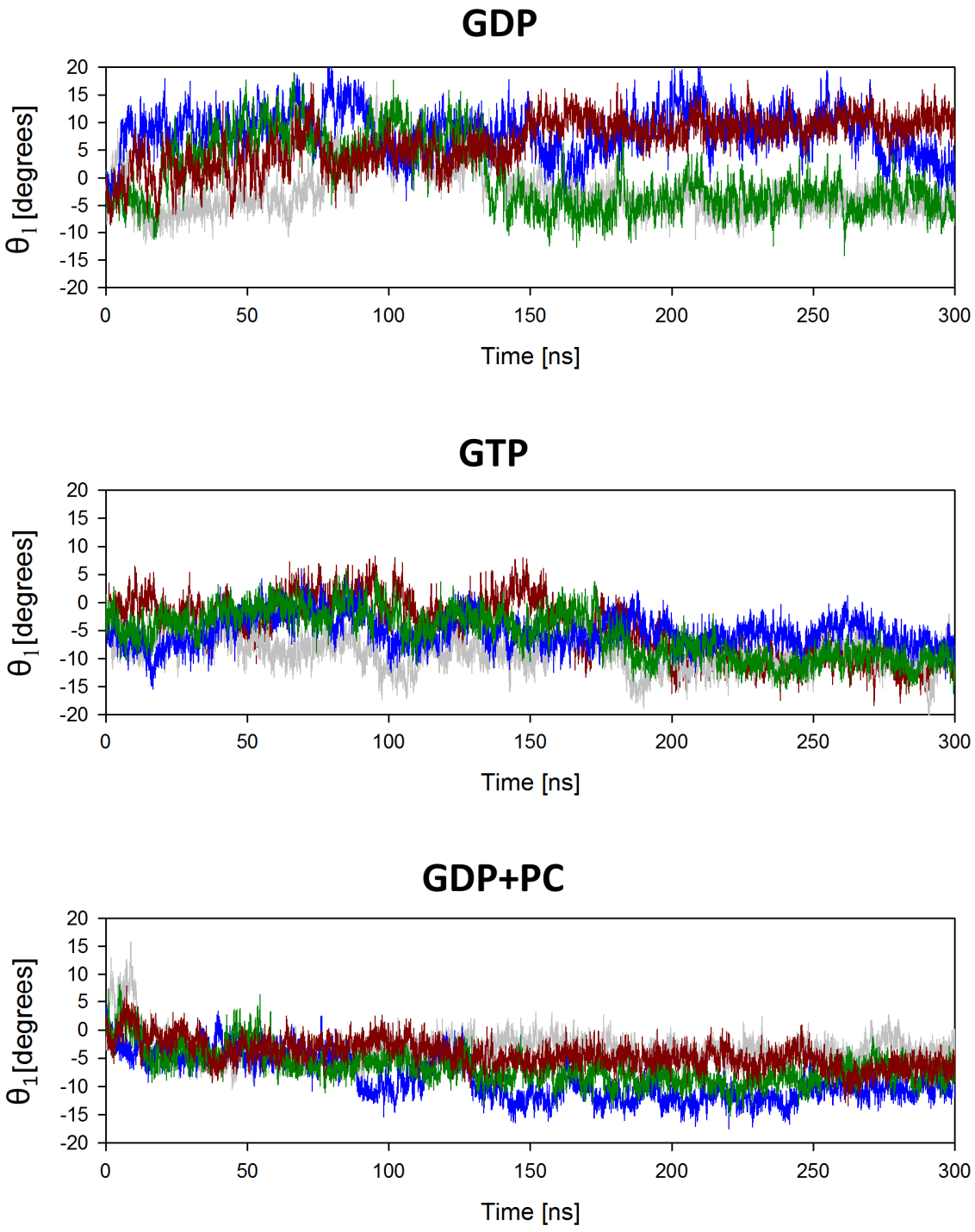

Figure S4. Time evolution of the main bending angle θ_1 for the four central interfaces of filament calculated as described in Fig. S3. Notice that the GDP-filament converges to heterogeneous filament formed by open (~6 degrees) and closed (~-6 degrees) interfaces. In contrast, the monomer association remains closed during all the simulations for GTP and GDP-bound filaments

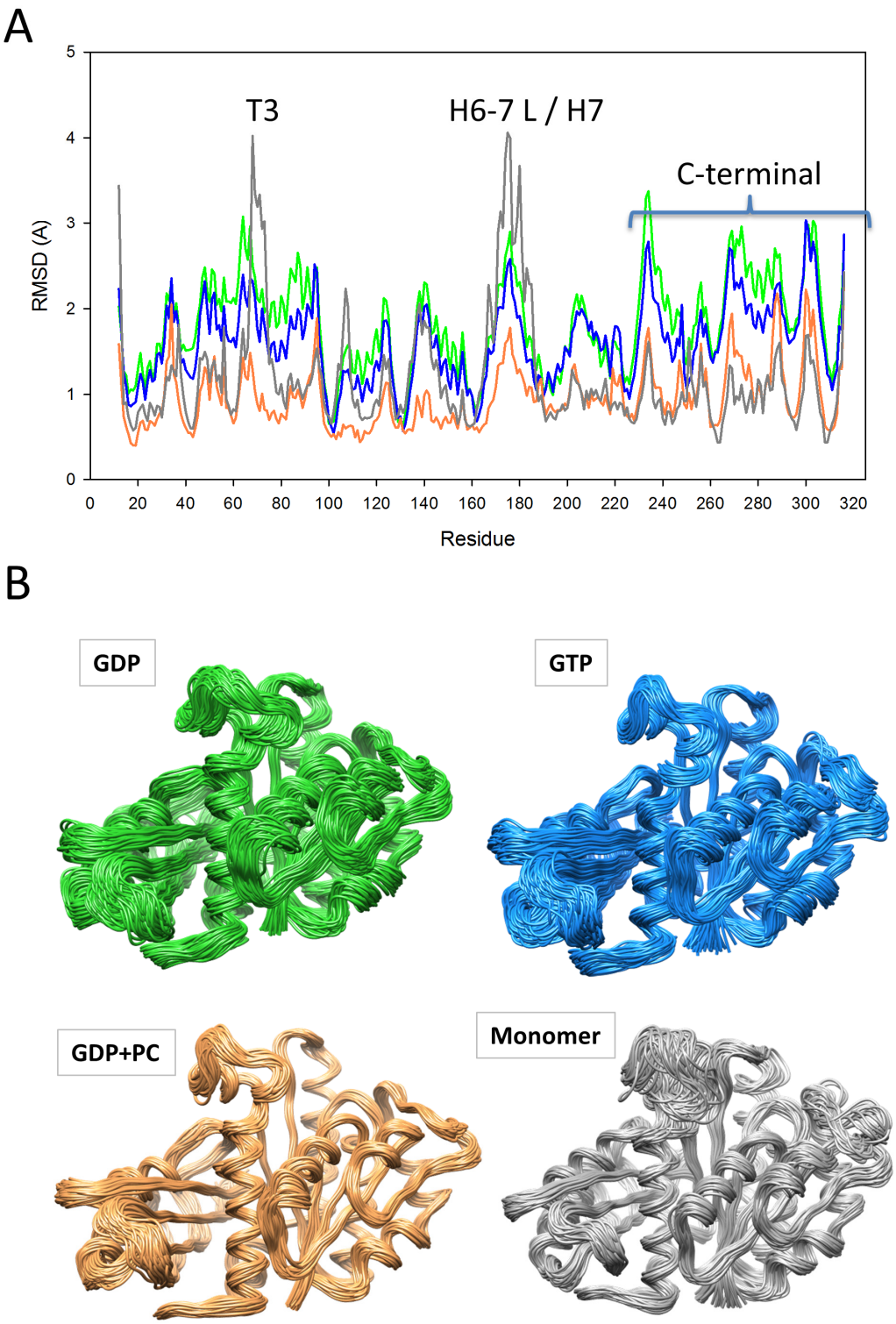

Figure S5. Average monomer conformations from the final 100 ns of the trajectories were aligned via a maximum-likelihood superimposition criterion using THESEUS (3) for the GDP filament (green), the GTP filament (blue), the PC filament (wheat) and an isolated GDP FtsZ monomer (gray). (A) Average RMSD per residue obtained from the superimposition. (B) Corresponding ensemble overlaps.

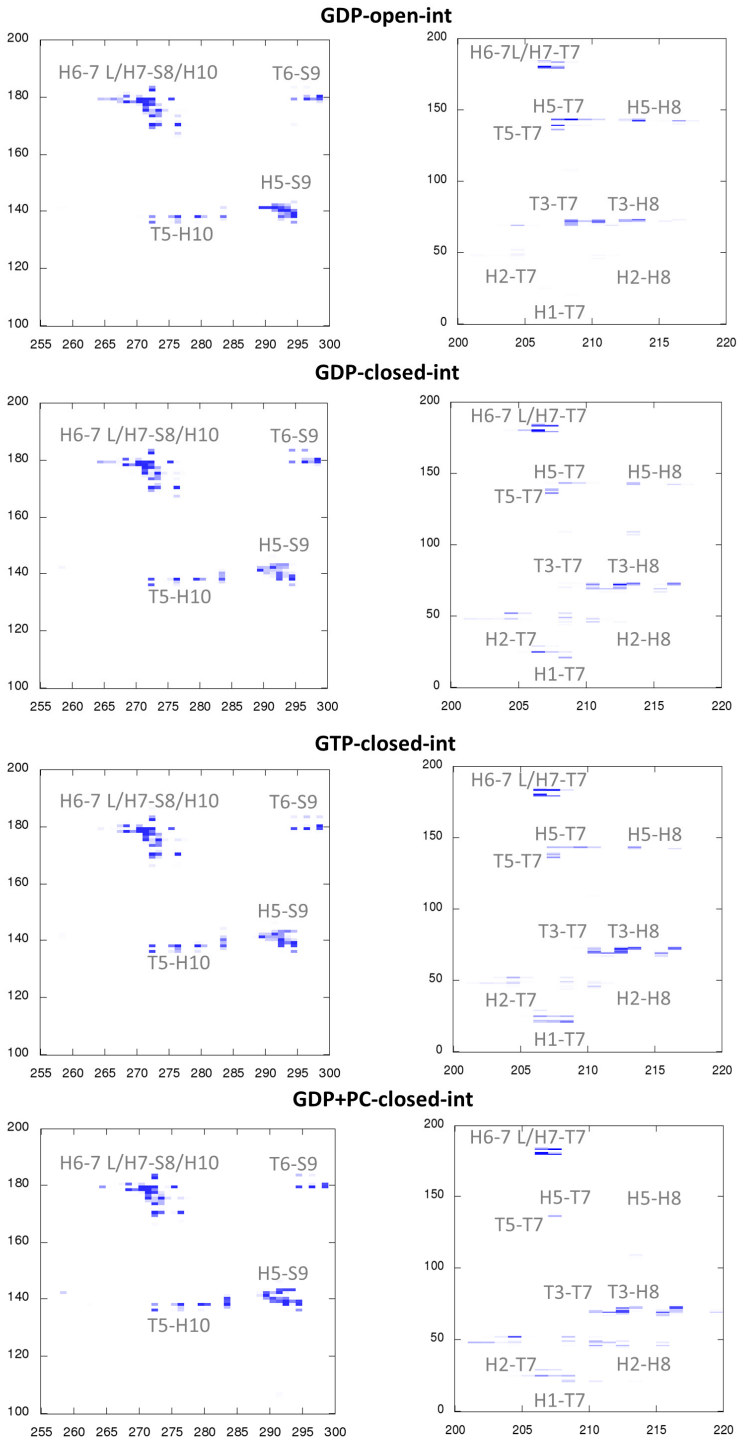

Figure S6. Contact plots of the monomer-monomer interfaces. Two residues were considered to be in contact if they had at least one pair of atoms separated by less than 4 Å. Contacts were calculated for the four central monomer interfaces throughout the final 100 ns of the simulations. The numbers in the axes are residue positions. The intensity of each band reflects the percentage of simulation time during which the contact was present. Dark blue regions correspond to contacts that were present throughout the entire simulation time. The relative differences between GDP and GTP contact patterns are detailed in the main text. In comparison to the simulations with bound GDP, the presence of PC stabilized the contacts of the top monomer's T7 loop with the bottom monomer's H2 and H1 helices and those

formed by H2-H8, and impeded the contacts of bottom H5 helix observed with other filaments. As shown by the crystal structure (4-6), the benzamide moiety makes the major contribution to the binding. During our simulations, the amide group formed stable H-bonds with Val207 (T7) and Asn263 (H8) and, in a more transient fashion, with Gly205 and Leu209. The thiazolopyridine part of the ligand interacted with the H7 helix (residues Gly193, Gly192 and Glu196) and with the C-terminal domain (residues Met226 and Ile228). Interestingly, the presence of PC impeded the contacts with the H5 helix disrupting the stable H-bonds of Asp-213 with Lys142 and Arg143 that were observed in the other filaments. By contrast, more stable contacts of the H2 helix with the T7 loop and the H8 helix were present; for example, the binding of Asp210 (T7) to the T3-loop glycine cluster observed in other cases was replaced by an interaction with Gln48 (H2).

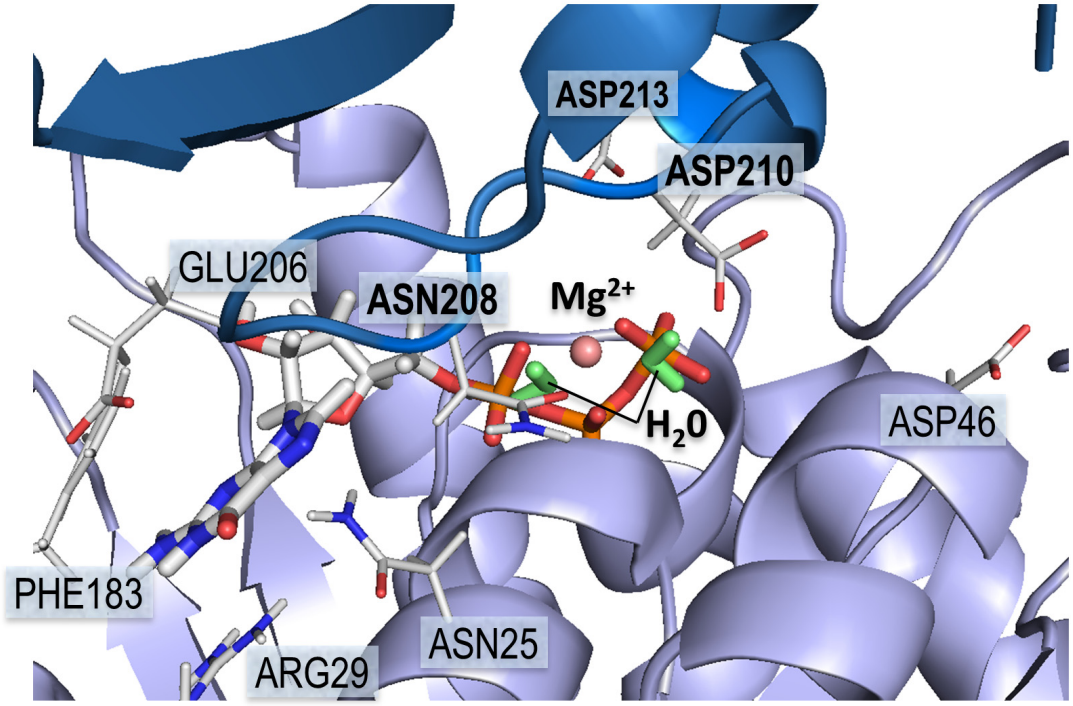

Figure S7. Detailed view of the GTP-filament interface. Among the elements of the Mg^{2+} coordination shell, the strongest interactions corresponded to the Asn208 from the T7 loop and to the β and γ phosphates (orange). The magnesium interactions held the binding pocket closed and stabilized the GTP nucleotide in a position suitable for hydrolysis. In this case, the carbonyl group of Asp210 is located at the correct hydrogen-bonding distance to polarize one of the water molecules (green) coordinated with the magnesium (pink).

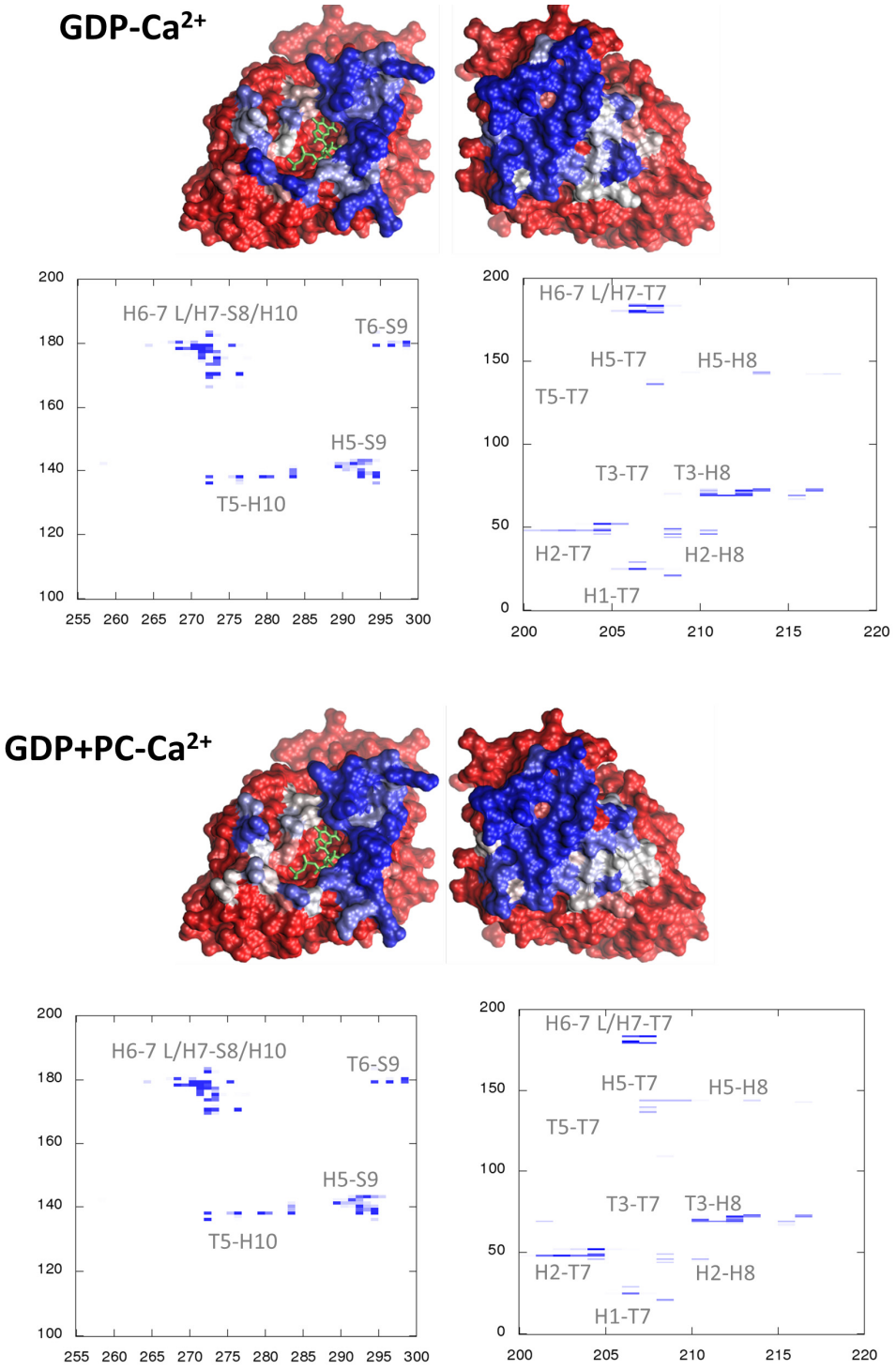

Figure S8. Contact surfaces and interface contact plots of the monomer-monomer interface for FtsZ filament simulations with a bound Ca^{2+} ion (see Fig. 3 and SI Fig. S6 for corresponding results without Ca^{2+}). In comparison to the simulations without calcium, there was an apparent increase in the inter-monomer contact near H2. As observed in the crystal structure, Ca^{2+} formed a coordination center with two water molecules inside the T7 loop. In our simulations, we found that the carbonyl groups of Leu200, Val203, Ser204, Asn280 and Asp210 were all located at compatible coordinating distances, but the Ca^{2+} ion interacted more closely with the latter two residues. Other important interactions were detected with either Asp46 or Gln48 at the H2 helix of the bottom subunit.

Movies

FtsZ_Movie 1. MD simulation trajectories of GDP-, GTP- and PC-bound filaments.

FtsZ_Movie 2. Animation of the transition among GTP, GDP-closed and GDP-open states. A feasible pathway was generated among the illustrative dimers extracted from the corresponding MD filament simulations. As in Fig. 1, the blue color represents GTP, cyan represents GDP-closed dimers, and green represents GDP-open dimers. The transitions were obtained using the normal-mode analysis in internal coordinates suite iMOD (7). Notice that the orientations of movie 1 (Fig. 1A) and movie 2 (Fig. 1B) are related by a rotation of 45 degrees around the axis of the filament.

FtsZ_Movie 3. MD simulation of the activation switch. The conformational change observed with a single SaFtsZ monomer during the transition from the open-cleft to the closed-cleft conformations. The movie includes the first 35 ns of the simulation.

Supporting References

1. Hsin J, Gopinathan A, & Huang KC (2012) Nucleotide-dependent conformations of FtsZ dimers and force generation observed through molecular dynamics simulations. *Proc Natl Acad Sci U S A* 109(24):9432-9437.
2. Grafmuller A & Voth GA (2011) Intrinsic bending of microtubule protofilaments. *Structure* 19(3):409-417.
3. Theobald DL & Wuttke DS (2008) Accurate structural correlations from maximum likelihood superpositions. *PLoS Comput Biol* 4(2):e43.
4. Matsui T, *et al.* (2012) Structural reorganization of the bacterial cell-division protein FtsZ from Staphylococcus aureus. *Acta Crystallogr Sect. D Biol Crystallogr* 68(9):1175-1188.
5. Tan CM, *et al.* (2012) Restoring methicillin-resistant Staphylococcus aureus susceptibility to β-lactam antibiotics. *Sci Transl Med* 4(126):126ra135.
6. Elsen NL, *et al.* (2012) Mechanism of action of the cell-division inhibitor PC190723: modulation of FtsZ assembly cooperativity. *J Am Chem Soc* 134(30):12342-12345.
7. Lopez-Blanco JR, Garzon JI, & Chacon P (2011) iMod: multipurpose normal mode analysis in internal coordinates. *Bioinformatics* 27(20):2843-2850.